Colloids and Surfaces B: Biointerfaces 185 (2020) 110542

Contents lists available at ScienceDirect

Colloids and Surfaces B: Biointerfaces

journal homepage: www.elsevier.com/locate/colsurfb

Hydroxyl radicals and oxidative stress: the dark side of Fe corrosion

E. Scarcello[a,*], A. Herpain[a], M. Tomatis[b], F. Turci[b], P.J. Jacques[c], D. Lison[a]

[a] Université catholique de Louvain, Louvain centre for Toxicology and Applied Pharmacology, LTAP, Avenue Hippocrate 57, 1200, Brussels, Belgium
[b] University of Torino, Department of Chemistry and "G. Scansetti" Interdepartmental Center for Studies on Asbestos and Other Toxic Particulates, Via P. Giuria 7, I-10125, Turin, Italy
[c] Université catholique de Louvain, Institute of Mechanics, Materials and Civil Engineering, IMAP, Place Sainte Barbe 2, Louvain-la-Neuve, B-1348, Belgium

ARTICLE INFO

Keywords:
Iron alloy
Corrosion
Oxidative stress
Hydroxyl radical
Catalase
Vascular cell

ABSTRACT

Fe-based materials are considered for the manufacture of temporary implants that degrade through the corrosion of Fe by oxygen. Here we document the generation of hydroxyl radicals ($HO^{\cdot}$) during this corrosion process, and their deleterious impacts on human endothelial (ECs) and smooth muscle cells (SMCs) *in vitro*. The generation of $HO^{\cdot}$ was documented by two independent acellular assays, terephtalic acid hydroxylation (fluorescence) and spin trapping technique coupled with electron paramagnetic resonance spectroscopy. All Fe-based materials tested exhibited a strong potential to generate $HO^{\cdot}$. The addition of catalase prevented the formation of $HO^{\cdot}$. Cellular responses were assessed in two ECs and SMCs lines using different cytotoxicity assays (WST-1 and CellTiter-Glo). Cells were exposed directly to Fe powder in the presence/absence of catalase, or to extracts obtained from the corrosion of Fe. Cell viability was dose-dependently affected by the direct contact with Fe materials, but not in the presence of catalase or after indirect exposure to cell extracts. The deleterious effect of $HO^{\cdot}$ on ECs and SMCs was confirmed by the dose-dependent increase of the transcripts of the oxidative stress gene *heme oxygenase-1* 4 h or 6 h after direct exposure to the particles, but not in presence of catalase or after indirect exposure. The demonstration of $HO^{\cdot}$ production during corrosion and consequent oxidative stress on human ECs and SMCs newly reveals a deleterious consequence of Fe-corrosion that should be integrated in the assessment of the biocompatibility of Fe-based alloys.

1. Introduction

Atherosclerosis is the dominant cause of cardiovascular diseases, accounting for the majority of human deaths worldwide [1]. One therapeutic option is the implantation of a stent in the diseased vessel, *e.g.* a coronary artery. Research into biodegradable stents has recently gained increasing attention because of their theoretical advantages over current permanent stents. Bioresorbable materials can temporally withstand artery recoil and then degrade 6–12 months after implantation, avoiding late adverse effects such as restenosis or thrombosis [2]. Bioresorbable stents can be made of different materials such as polymers or metals. Among metals, Fe-based alloys have emerged as potentially useful materials due to their excellent mechanical properties that combine high strength with uniform elongation, together with a progressive corrosion in biological tissues [3].

A material for cardiovascular implantation should also be biocompatible, *i.e.* as inert as possible, without causing inflammation, neointimal proliferation, thrombotic events, material overload, local toxicity or abnormal clinical observations; and it should also guarantee a complete integration with the surrounding tissue [4].

Previous *in vivo* studies on Fe-based implants did not show overt local cytotoxicity, inflammation, thrombosis or early restenosis [5–9]. However, most authors documented the accumulation of degradation products 9–12 months after stenting in a rat or rabbit model. These products were identified at the junctions of the stent struts as clusters or voluminous flakes, that both localized to and extended away from the stent surface [5,6,10]. The accumulation of massive corrosion products repelled neighboring cells and tissues, and reduced the vessel lumen due to excessive intimal hyperplasia. The exact mechanism of this phenomenon has not been elucidated [11].

Accordingly, *in vitro* studies have mainly considered that products formed and released from degradable Fe-containing materials drive cytotoxicity. Thus, the biocompatibility of metal stent components has generally been assessed in cells exposed to soluble or degradation products of Fe-based materials [11]. *In vitro* results in endothelial (ECs), smooth muscle cells (SMCs) or fibroblasts largely indicated good cytocompatibility for eluates from Fe-based materials [12–16].

Lin *et al.* [17] firstly observed that small corrosion particles from

* Corresponding author.
E-mail address: eleonora.scarcello@uclouvain.be (E. Scarcello).

https://doi.org/10.1016/j.colsurfb.2019.110542
Received 19 July 2019; Received in revised form 7 September 2019; Accepted 1 October 2019
Available online 24 October 2019
0927-7765/

bioresorbable Fe-based materials induced cytotoxicity in fibroblasts *in vitro*. Recently, Fagali *et al.* [18] examined the biological impact of soluble and insoluble corrosion products released by Fe (Fe-microparticles or bulk Fe) on adjacent fibroblasts. They showed that insoluble Fe corrosion products were associated with cytotoxicity and intracellular reactive oxygen species (ROS) whereas soluble corrosion products did not affect cell viability [19]. However, the exact chemical species released from native Fe that cause this cytotoxicity are unknown. Therefore, the aim of this study is to elucidate the mechanism behind the cytotoxicity of Fe-based materials, in both ECs and SMCs, which are the most relevant cell types surrounding the stent during the largest part of its lifetime. We argued that as Fe corrosion is driven by dissolved oxygen, Fe^{2+} ions and hydrogen peroxide (H_2O_2) are formed and can participate together in a Fenton reaction generating hydroxyl radicals (HO•) as described in reaction (1) below:

$$Fe^{2+} + H_2O_2 \rightarrow Fe^{3+} + HO\bullet + OH^- \quad (1)$$

Hydrogen peroxide implicated in the Fenton reaction can be generated by different mechanisms. Under acidic conditions, Fe reacts with oxygen to produce hydrogen peroxide through a two-electron transfer as indicated in reaction (2) [20]:

$$Fe + O_2 + 2H^+ \rightarrow Fe^{2+} + H_2O_2 \quad (2)$$

At neutral pH the dominant source of H_2O_2 implicates the generation of the intermediate superoxide anion ($O_2\bullet^-$). Ferrous iron produced by Fe oxidation reacts with oxygen through a series of one-electron transfers to produce H_2O_2 according to the following reactions (3)–(5) [21]:

$$Fe \rightarrow Fe^{2+} + 2e^- \quad (3)$$

$$Fe^{2+} + O_2 \rightarrow Fe^{3+} + O_2\bullet^- \quad (4)$$

$$Fe^{2+} + O_2\bullet^- \rightarrow Fe^{3+} + H_2O_2 \quad (5)$$

In both cases, H_2O_2 ultimately reacts with ferrous iron *via* a Fenton reaction to produce HO• [22].

The high reactivity of HO• produced from the corrosion of Fe particles is used *e.g.* to remove pollutants in water and wastewater treatment [23]. Thus, since HO• are capable of extensively degrading organic contaminants in a variety of biological systems, it appears plausible that the corrosion of Fe-based implants might have a deleterious impact on vascular cells.

In the present work we postulated that HO• represent the critical specie resulting from Fe corrosion that could contribute to adversely affect vascular cells. We considered that because of their nonselective behavior and rapid reactivity with numerous molecules, HO• can only affect cells in direct contact with the implant. Therefore, the potential toxic contribution of HO• might not be captured in assays using corrosion extracts collected after the corrosion of the same materials. Thus, we compared the effects of direct exposure to Fe and indirect exposure to extracts.

2. Materials & methods

2.1. Metallic materials

Several Fe-based materials differing in their composition or shape were tested. Carbonyl iron powder with > 99.5% purity was provided by Sigma-Aldrich (St Louis, MO). The size of the spherical particles of iron ranged from 5 to 9 µm as illustrated by the scanning electron microscopy micrographs on Fig. S**1**. Commercial bars, 15 mm in diameter, of 316 L stainless steel grade were gas atomised. Induction drip-melting of these bars was used to melt the alloy. The liquid was then atomised owing to high pressure Ar. The resulting powder was then sieved in 3 steps. The first one removed big particles above 120 µm. Sieving down to 70 µm and then 20 µm was then carried out. Resulting particles had a median size of 15 µm. Sheets of pure iron (> 99.99% purity) were manufactured, starting from the arc-melting of chunks (from Alfa Aesar, Tewksbury, MA). The resulting ingot was then annealed at 1000°C for 10 min and hot-rolled down to a thickness close to 2 mm. Fe-22Mn-0.6C (in wt.%) alloy, known as a TWIP steel (for twinning-induced plasticity [24] was also tested, as sheet, 1 mm in thickness. This sheet was obtained after hot and cold rolling followed by annealing at 900°C [25]. 10 x 10 mm samples were then machined from the sheets. Both sides of the sheet samples were wet-grinded from 320 grit SiC water-proof paper down to 1 µm diamond paste and then rinsed with 99.8 vol% absolute ethanol. The sheet specimens were ultrasonically washed in absolute ethanol for 10 min immediately before HO•-generation tests. Rough square sheet samples were also used for HO•-release assay.

2.2. Spin trapping technique

The ability of the different samples to generate HO• was investigated by using a target molecule (formate ion) that reacts with HO• leading to carbon-centered radicals ($CO_2\bullet^-$). $CO_2\bullet^-$ are subsequently trapped by a spin trap molecule (DMPO) and the stable adduct is detected by electron paramagnetic resonance spectroscopy. Fe particles (75 mg) or square massive sample (Fe or TWIP steel sheets) were suspended in 1 ml of phosphate buffer (PB, 0.5 M, pH 7.4, Sigma-Aldrich, Milan, Italy) containing sodium formate (1.0 M, Sigma-Aldrich, Milan, Italy) and DMPO (0.04 M, Cayman Chemical Company, Ann Arbor, Michigan). After 10, 30 and 60 min of incubation under continuous stirring, aliquots of 50 µl were withdrawn, filtered (cellulose acetate filters, pore diameter 0.22 µm, Merck Chemicals SA, Tullagreen, Carrigtwohill, Co. Cork, Ireland) and EPR spectra were recorded at room temperature with a Miniscope MS 100 EPR spectrometer (Magnettech, Berlin, Germany). The instrument settings were as follows: modulation 1000 mG, scan range 120 G, center of field approximately 3355 G. Blanks were run in parallel in the absence of sample. All the measurements were performed in triplicate.

2.3. Fluorimetric determination of hydroxyl radicals

To confirm EPR results, HO• were measured through the disodium terephthalate (TA, 99%, Alfa Aesar, Tewksbury, MA) assay. TA reacts with HO• to form 2-hydroxyterephthalic acid that gives a bright stable fluorescence. TA was dissolved in 0.01 M PBS (pH 7.4) at a final concentration of 10 mM [26]. Fe particles or square sheet samples were suspended in TA solution (30 mg of powder or 10 x 10 mm metal square sheet/ml) and incubated for 30 min at 25°C under continuous stirring. In some assays, catalase (1000 U/ml, Sigma-Aldrich, St Louis, MO) was added to the reaction mixture. After incubation, the suspensions were filtered on cellulose acetate membrane (0.22 µm) and the fluorescence of the filtrate was measured at $\lambda_{em} = 425nm$ on a SpectraMax i3x Multi-Mode microplate reader with an excitation light $\lambda_{ex} = 324nm$.

The role of soluble molecular oxygen (O_2) in HO• generation was verified for both procedures (EPR and TA). In these assays, the aqueous buffered solution containing DMPO and sodium formate or TA was deoxygenated by bubbling N_2 for 30 min before adding samples and throughout the duration of the tests.

2.4. Cell culture

Cell studies were performed with ECs (Human Umbilical Vein, HUVECs, and Human Aortic, HAoECs; Cell Application, Sigma-Aldrich, San Diego, CA) and SMCs (Human Coronary Artery, HCASMCs, and Human Aortic, HAoSMCs; Cell Application, Sigma-Aldrich, San Diego, CA) because both cell types are in direct contact with the stent surface immediately after implantation [19]. ECs were cultured on 0.2% gelatin-coated 75-cm^2 culture flasks (Corning Incorporated, Corning, NY) in Endothelial Cell Growth Medium (Cell Application, Sigma-Aldrich, San Diego, CA) whereas SMCs were grown on 75-cm^2 culture flasks

with Human Smooth Muscle Cell Growth Medium (Cell Application, Sigma-Aldrich, San Diego, CA); both maintained in a humidified incubator (New Brunswick Galaxy® 170S) containing 5% CO_2 at 37°C. Cells were grown to confluency and harvested by trypsinization. A maximum of 7 (HUVECs) and 5 (HAoECs, HCASMCs and HAoSMCs) passages was used to maintain phenotypic cell characteristics. Cells were also routinely tested for the absence of Mycoplasma infection (PCR Mycoplasma Test Kit I/RT, PromoKine, Huissen, the Netherlands).

2.5. SMCs differentiation

Proliferative SMCs were cultured for 10 days in a 96-well plate with a human smooth muscle cell differentiation medium (311D, Sigma-Aldrich, San Diego, CA). The differentiation to contractile phenotype was verified by *α-actin* and *calponin* mRNA expression (see below).

2.6. Cell viability assays

Particles were heated at 200°C (WTB, Binder® drying oven) during 2 h to sterilize the material and inactivate any possible endotoxin contamination immediately before cell exposure. The particles were next suspended in cell culture medium at a stock concentration of 5 mg/ml and diluted to final concentrations in culture medium and vortexed. Cells were also exposed to corrosion extracts generated after immersion of increasing concentrations of Fe particles in cell culture medium for 24 h and centrifugation. The concentration of soluble Fe ions was quantified by inductively coupled plasma - mass spectroscopy (ICP-MS) after filtration of the suspension (Amicon® 5000 NMWL, Millipore Corporation, Bedford) (Fig. S**2**).

Cell viability was assessed with the colorimetric WST-1 assay from Roche Diagnostics GmbH (Mannheim, Germany) and the luminescent CellTiter-Glo® 2.0 assay from Promega Corp. (Madison, WI). In the WST-1 assay, the amount of formazan dye formed is directly related to the number of metabolically active cells. The assay was carried out as described in the manufacturer's instructions. In brief, cells (2.10^4 ECs or 10^4 SMCs) were seeded in 96-well transparent plates and exposed the day after to different concentrations of Fe particles or equivalent extracts for 24 h. Cells were then washed and incubated in fresh medium with 10% WST-1 reagent for 2 h. Absorbance was measured at 450 nm, with 690 nm as reference, in a multiplate reader (Infinite F200, Tecan®). Results are reported as relative WST-1 activity, where 1.0 corresponds to the absorbance measured in control cultures. The CellTiter-Glo® 2.0 assay determines the number of viable cells in culture by quantitating the amount of ATP in metabolically active cells. In brief, cells were seeded in 96-well white plates and exposed as above. After 24 h, the CellTiter-Glo® reagent was added and luminescence was read on a luminometer (Victor™ X4, PerkinElmer®). Results are reported as for WST-1. We verified that Fe, at the dose ranges tested, did not interfere with the WST-1 and CellTiter-Glo® 2.0 assays (not shown). Min-U-Sil® 5 (ECs) or Rotenone (SMCs) were used as positive cytotoxic controls.

2.7. Gene expression experiments

We considered that if oxidative damage is responsible for the cytotoxic activity of Fe powder measured at 24 h, oxidative stress should be detected at an earlier time point. ECs or SMCs were exposed to increasing concentrations of Fe or extracts for 4 h or 6 h with/without catalase (1000 U/ml) to document the expression of the oxidative stress response gene heme oxygenase-1 (*HO-1*). Reverse transcription and quantitative polymerase chain reaction (RT-PCR) for *HO-1* were performed following the protocol supplied by Roche (Mannheim, Germany). First-strand cDNA synthesis was performed with 13.5 µl of RNA adjusted to a concentration of 5 ng/µl. RT mix containing reaction buffer and enzyme mix was added to the samples and incubated at 37°C during 1 h followed by a step of heat-inactivation at 70°C for 15 min. Amplified DNA fragments from HUVECs exposed to 5 µM of Sodium (meta)arsenite (Merck, Saint Louis, MO) were purified and quantified from a 1.5% agarose gel with Nucleospin Extract (Macherey-Nagel, Düren, Germany) and then serially diluted to serve as standards in real-time PCR. For the quantitative PCR, samples were diluted 10-fold in sterile UltraPure® water (Invitrogen), and 5 µl were loaded in 96-well PCR plates. PCR master mix and PCR primers set were added (total volume: 20 µl), and PCR was performed in on a StepOnePlus™ Real-Time PCR System Thermal Cycling Block (Applied Biosystems, Foster City, CA) following the kit protocol. Sequences of interest were amplified using the following forward: 5′ G CAA CAA AGT GCA AGA TTC TGC 3′ (*HO-1*); 5′ CC CGT GCT GCT GAC CGG 3′ (*β-actin*); and reverse primers: 5′ G CTG TAG GGC TTT ATG CCA TGT 3′ (*HO-1*); 5′ C GTC ACC GGA GTC CAT CAC 3′ (*β-actin*). After amplification, a melting curve was generated to check that the amplified double-stranded DNA products are a single discrete species and data analysis was performed with the StepOne™ Software v2.3 (Applied Biosystems). Results were calculated as fold increase of *HO-1* expression to the expression of the housekeeping gene *β-actin*.

For the characterization of the contractile SMCs, the following forward and reverse primer sequences were used: 5′ G ACG AAG CAC AGA GCA AAA GAG 3′ (FP *α-actin*); 5′ A GAA CAA GCT GGC CCA GAA GTA 3′ (FP *calponin*); 5′ A GAG TGG TGC CAG ATC TTT TCC 3′ (RP *α-actin*); 5′ TT GAG GCC GTC CAT GAA GTT 3′ (RP *calponin*).

2.8. Blocking hydroxyl radical generation

In order to block HO• generation, *in vitro* experiments were repeated in the presence of catalase (1000 U/ml, Sigma-Aldrich, St Louis, MO). Some experiments were repeated using bovine serum albumin (BSA, Sigma-Aldrich, St Louis, MO) instead of catalase to exclude a potential non-specific effect, *e.g.* by protein adsorption on the particle surface.

2.9. Statistical analysis

Values are presented as means ± standard error of the mean (S.E.M.) of independent experiments (N) conducted in replicates (n). The data were analyzed with GraphPad Prism (GraphPad software, La Jolla, CA) or Origin software (OriginLab Corp., Northampton, MA). Differences between groups were analyzed by one-way analysis of variance (ANOVA) followed by a post-hoc Dunnett's pairwise comparison test or linear trend test. Differences with p value < 0.05 were considered statistically significant.

3. Results

3.1. Corrosion of Fe-based materials generates hydroxyl radicals

First, the formation of HO• during the corrosion of Fe-based materials was documented by monitoring the formation of carbon-centered free radicals in the presence of formate anions [27]. The cleavage of the C—H bond by HO• was detected by spin trapping and quantified by EPR spectroscopy. Representative EPR spectra of the [DMPO–CO_2]•– adducts indicate that Fe powder (Fig. 1b), Fe square sheet (Fig. 1c) and TWIP steel square sheet (Fig. 1d) strongly generate HO• in solution. No signal was detected in the absence of Fe (blank) (Fig. 1a). The strong activity of Fe-based materials was maintained for up to 60 min.

In order to support EPR results, we applied a complementary test using a different readout, *i.e.* the capacity of HO• to hydroxylate TA. Compared to the blank (Fig. 2), all Fe-based samples were able to hydroxylate TA, regardless of their weight, form, composition or polishing (similar results were obtained with rough or 1 µm polished Fe square sheets, not shown). The specificity of the TA measurement was verified by adding catalase, which significantly reduced the signal, which is consistent with the generation of HO• during Fe-based materials corrosion.

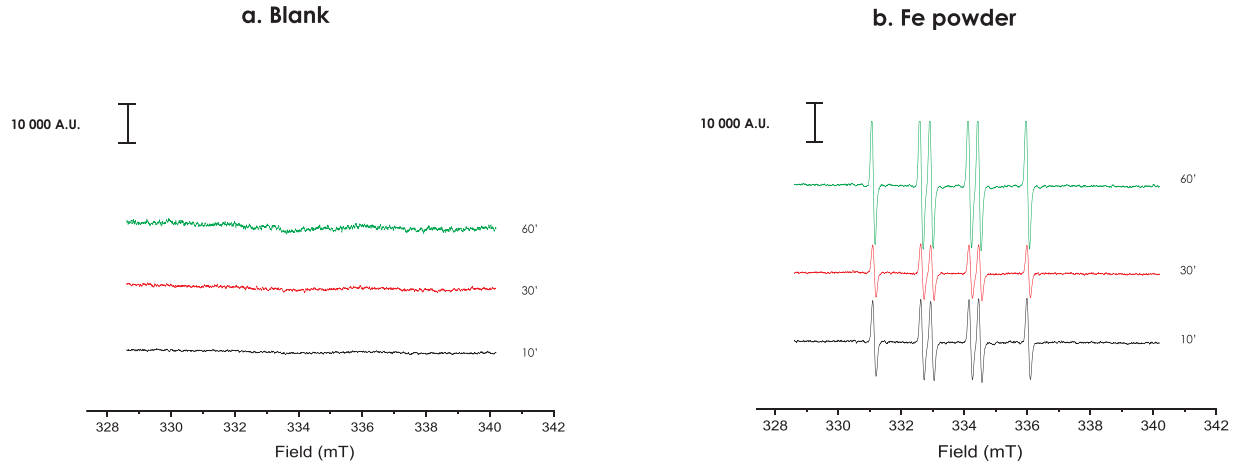

Fig. 1. Surface driven release of HO• from the corrosion of Fe-based materials. EPR spectra recorded on suspensions of Fe powder (75 mg, **b**), Fe square sheet (10 × 10 x 1.5 mm, **c**) and TWIP steel square sheet (10 × 10 x 1.5 mm, **d**) compared to blank (**a**) in a sodium formate-buffered solution in the presence of DMPO as spin-trapping agent at RT. Aliquots of 50 µl of suspension were withdrawn after 10, 30 and 60 min of incubation under continuous stirring at room temperature, filtered and analyzed for EPR spectra. The panel shows a representative spectrum out of at least three determinations.

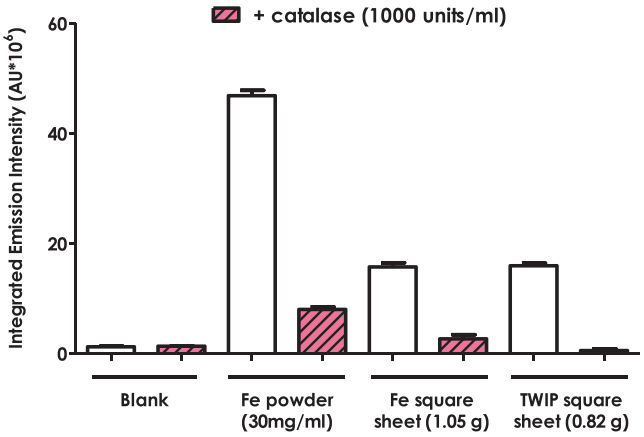

Fig. 2. Corrosion of Fe-based materials generates HO•. Fluorimetric determination of HO• released from Fe-based materials using the terephthalate (TA) assay. Samples were immersed in a buffered (PBS) solution of disodium terephtalate (10 mM) for 30 min at RT under continuous stirring. In parallel experiments, catalase (1000 U/ml) was added during incubation. Supernatant was recovered, filtered and fluorescence was measured (excitation λ_{ex} = 324 nm, emission λ_{em} = 425 nm). Values are means ± SEM (N = 2, n = 3).

To confirm that dissolved oxygen drives the generation of HO•, spin trapping and fluorimetric TA measurements were performed in deoxygenated solutions. The absence of oxygen completely suppressed the corrosion mechanism and consequently the generation of HO• (not shown).

3.2. Direct cellular contact with Fe corrosion induces ECs and SMCs cytotoxicity

The responses to Fe particles or extracts were compared in cytotoxicity assays, hypothesizing that only the direct contact with Fe particles could capture the cytotoxic activity of HO•. Experiments were carried out in endothelial (HUVECs and HAoECs) and proliferative smooth muscle (HCASMCs and HAoSMCs) cells lines using two cytotoxicity tests based on different principles (readouts), *i.e.* mitochondrial dehydrogenases (colorimetry) and ATP content (luminescence). Both assays showed that direct contact with Fe significantly and dose-dependently affected the viability of both cell lines after 24 h exposure (Fig. 3). ECs and SMCs did not show major difference in terms of sensitivity to Fe. In contrast, corrosion extracts did not exert a cytotoxic activity. In order to exclude a possible non-specific particle effect, we also exposed ECs and SMCs to a non-corrodible metallic powder. Stainless steel 316 L did not show any cytotoxic activity in endothelial cells using particles or extracts (Fig. S**3**), supporting a specific cytotoxic activity associated with Fe corrosion.

Since SMCs can show a contractile or a proliferative phenotype, cells were differentiated *in vitro* from the proliferative to the contractile phenotype. Differentiation was characterized by measuring the mRNA expression of *α-actin*, a major constituent of the contractile apparatus, and *calponin*, a regulator of SM contractility (Fig. S**4**). Cytotoxicity was assessed after direct exposure to Fe or corrosion extracts. Direct contact with Fe, but not corrosion extracts, induced cytotoxicity of a similar severity than in proliferative SMCs (Fig. 4).

To further support the role of HO• in the response of ECs and proliferative SMCs to Fe corrosion, the oxidative stress response was documented by monitoring the expression of heme oxygenase-1 *(HO-1)* after 4 h or 6 h exposure, *i.e.* before the occurrence of cytotoxicity. *HO-1* transcripts increased dose-dependently after Fe exposure, whereas corrosion extracts did not induce such a response (Fig. 5). The 316 L powder did not induce any oxidative stress response in endothelial cells (Fig. S**5**).

3.3. HO• released during Fe corrosion affect ECs and SMCs viability and induce oxidative stress

In order to demonstrate the implication of HO• in the cytotoxicity and oxidative stress response, we blocked HO• production with catalase. Catalase fully protected cells from the cytotoxicity (Fig. 6) and oxidative stress (Fig. 7) generated during Fe corrosion. Neither ECs (Figs. 6 and 7**a**, **b**) nor SMCs (Figs. 6 and 7**c**, **d**) were affected by Fe exposure in the presence of catalase, and the expression of *HO-1* was not upregulated in the presence of the enzyme, which is consistent with the implication of HO• in the cytotoxic and oxidative stress responses to Fe corrosion. HUVECs directly exposed to Fe in the presence of albumin instead of catalase showed a dose-dependent cytotoxicity (not shown), excluding a nonspecific effect of catalase, *e.g.* by protein adsorption on the particle surface.

4. Discussion

4.1. Experimental design

To cover a wide range of implanted materials used in medicine and their different surface reactivity, several samples of Fe-based materials

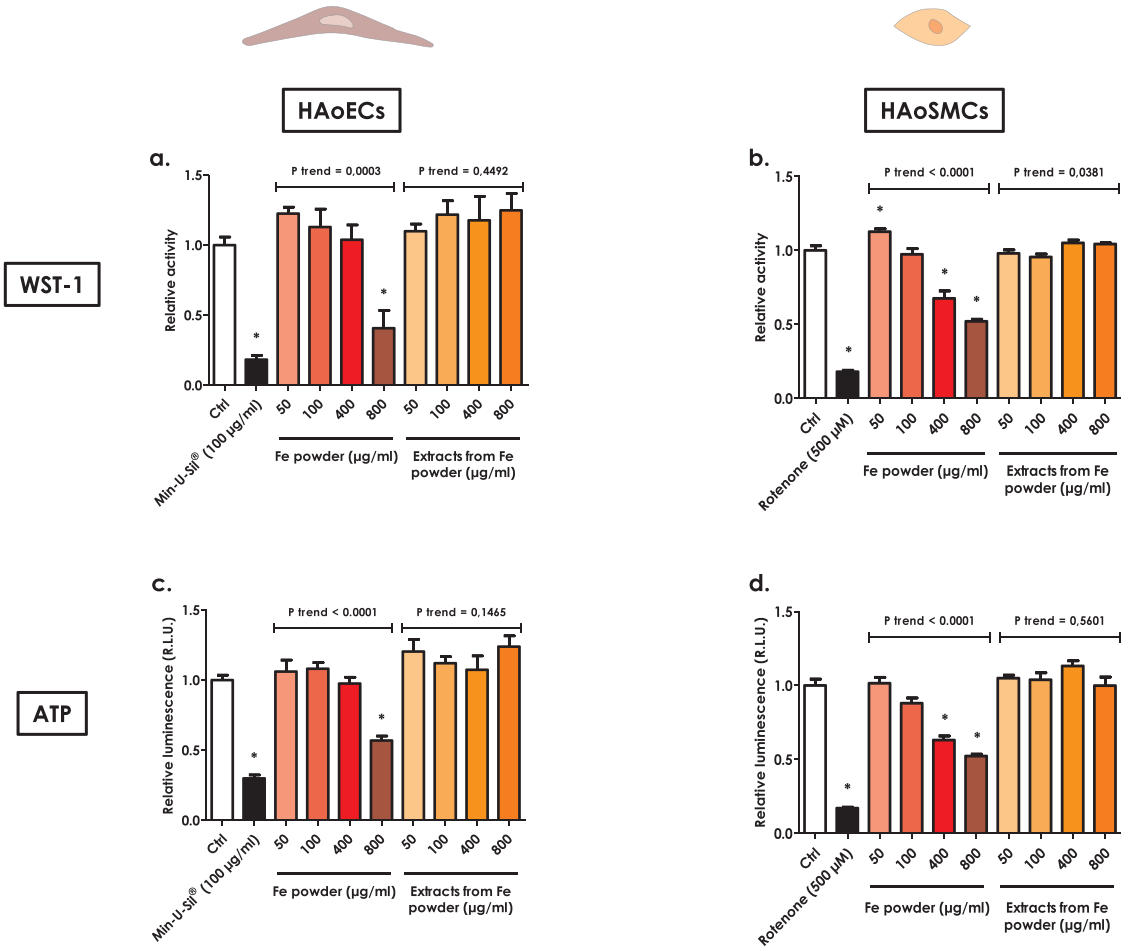

Fig. 3. Direct exposure to Fe powder affects ECs and SMCs viability. ECs or SMCs were seeded in 96-well transparent or white plates and exposed the next day to different concentrations of Fe powder or corrosion extracts for 24 h. Extracts were obtained from culture medium incubated during 24 h with increasing concentrations of Fe powder; supernatants were collected and centrifuged before cells exposure. The cells were washed and further incubated in fresh medium with 10% WST-1 reagent for 2 h. Absorbance was measured at 450 nm, with 690 nm as reference, in a multiplate reader (**a**: HUVECs; **b**: HAoECs; **c**: HCASMCs; **d**: HAoSMCs). The white plate was replenished with fresh medium containing the CellTiter-Glo® reagent (ATP) and luminescence was read (**e**: HUVECs; **f**: HAoECs; **g**: HCASMCs; **h**: HAoSMCs). Results are reported as relative WST-1 activity or luminescence, where 1.0 corresponds to the value measured in control cultures. Rotenone or Min-U-Sil® 5 were used as positive controls. Values are means ± SEM (N = 4, n = 4), $*p < 0.05$ relative to control. The trend analysis included controls.

differing in shape, size, surface area, roughness and composition were tested for their capacity to generate HO•. The surface reactivity of the metal square sheets was tested from rough to polished state (until 1 µm with diamond paste). All Fe-based samples examined here, in spite of their heterogeneity, showed a strong ability to generate HO• in acellular systems using two complementary techniques (EPR and TA hydroxylation assays). Any quantitative comparison of HO• yield among samples must, however, be carefully considered because samples were not tested under similar conditions of dose, surface area, geometry and Fe content.

We selected Fe particles as test material for cell experiments because, contrary to massive materials, they are compatible with most cytotoxicity assays, including WST-1 and CellTiter-Glo. They also allow for varying the dose and visualizing cells. The Fe samples used here are coated by a film of surface oxide, already formed directly after synthesis due to contact with atmospheric oxygen [28]. Therefore, although theseis material is generally referred as zerovalent metallic iron, Fe is covered by a nanometric layer of surface oxide/hydroxide. HO• generation is thus a balance between Fe leaching and the Fe surface oxide/hydroxide layer formation, which are competitively influencing each other [29]. EPR and TA hydroxylation results confirmed that the tested materials, despite their surface oxide layer, have a strong potential to generate HO•. This mechanism is specific to Fe, as confirmed by the protective role of catalase and by the absence of signal when using the stainless steel 316 L powder.

The impact of Fe particles and their degradation products were initially tested on ECs lines. These cells are of particular interest for endovascular stent application, as the endothelium is the first layer of cells in contact with the metallic stent during implantation and it also plays an important role shortly thereafter during re-endothelialization [30]. Cell viability and gene expression experiments were also performed on SMCs lines. This cell type may be of significance later in the healing process, when SMCs with a proliferative phenotype contribute to neointimal hyperplasia and, if left unchecked, to in-stent restenosis [31]. Cell viability was also measured on contractile SMCs, which represent the normal quiescent phenotype of these cells before the shift to the proliferative one after vessel injury [32].

4.2. Role of HO• in cytotoxicity and oxidative stress response

We compared here the response of human ECs and SMCs upon indirect or direct exposure to Fe particles. The first model assesses the impact of degradation products (*e.g.* Fe^{3+} ions), whereas the second one captures the effects of surface chemistry (including HO•) along with degradation products. We showed that only the direct contact between the Fe material and cells, and not degradation products, caused deleterious responses in ECs and SMCs through the HO• release. Indeed, catalase was able to protect both ECs and SMCs from oxidative stress

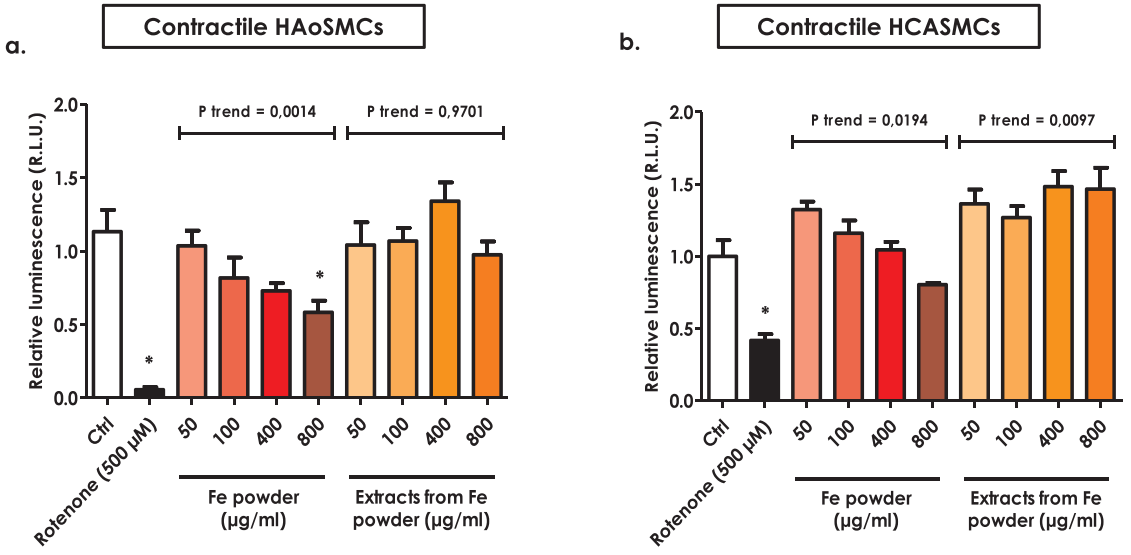

Fig. 4. Direct exposure to Fe powder affects contractile SMCs viability. Proliferative SMCs were seeded in 96-well white plates and cultured for 10 days with the differentiation medium. After differentiation to the contractile phenotype, HAoSMCs (**a**) or HCASMCs (**b**) were exposed to different concentrations of Fe powder or corrosion extracts for 24 h. Extracts were obtained from culture medium incubated during 24 h with increasing concentrations of Fe powder; supernatants were collected and centrifuged before cell exposure. The cells were washed and further incubated in fresh medium with the CellTiter-Glo® reagent and luminescence was read. Results are reported as relative luminescence, where 1.0 corresponds to the value measured in control cultures. Rotenone was used as positive control. Values are means ± SEM (N = 2, n = 4), $*p < 0.05$ relative to control. The trend analysis included controls.

and cytotoxicity, demonstrating that the deleterious effects were induced by HO• and not by degradation products (unaffected by catalase).

These data are consistent with the results reported by Fagali *et al.* [18] who explored the processes occurring at the Fe-biomaterial/cells interface and demonstrated that cell viability is not affected by high concentrations of soluble Fe, but is associated to the formation of insoluble products. This work demonstrates that complex events occur around Fe-based materials in contact with biological media and the distance between material and cells is crucial to interpret the biological impact of Fe corrosion. To some extent, these findings could also explain why a very large number of previous studies on the cytocompatibility of Fe or Fe-based implants, based mainly on indirect contact tests, showed very low alteration of cell viability [12,33–36]. These authors did, however, not provide an explanation for their observation.

It has already been highlighted that metallic Fe materials undergo electrochemical corrosion, which releases products of degradation at the implanted site thus generating ROS, such as HO• formed through the Fenton reaction with H_2O_2 [36]. However, little is known about the biological effects of this oxidant produced by metal degradation on the

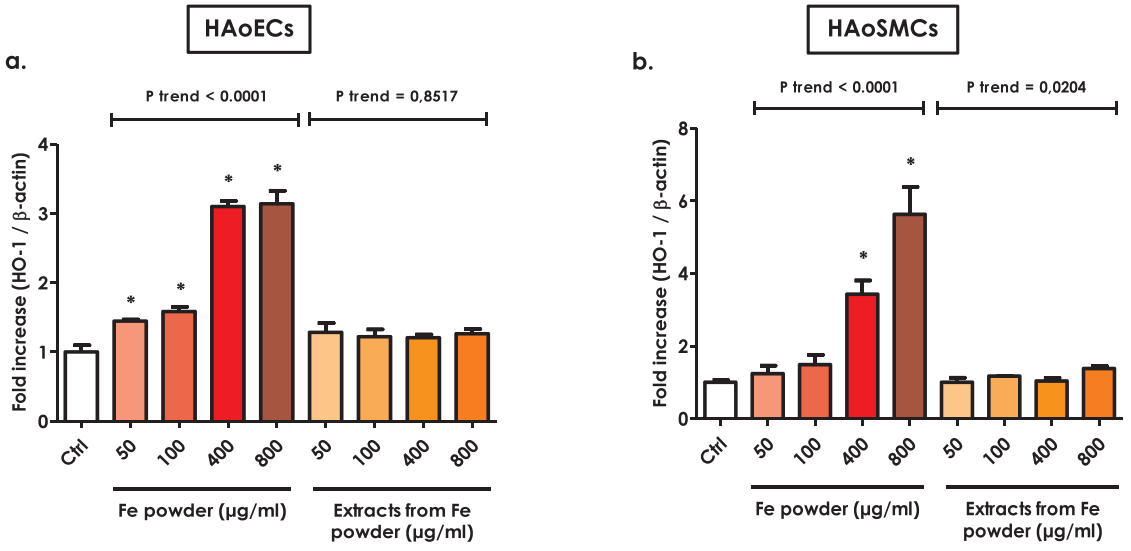

Fig. 5. Corrosion of Fe powder induces oxidative stress in ECs and SMCs. ECs (**a**: HUVECs; **b**: HAoECs) or SMCs (**c**: HCASMCs; **d**: HAoSMCs) were exposed to different concentrations of Fe powder or corrosion extracts for 4 h (ECs) or 6 h (SMCs). RNA was extracted and reverse transcribed for real-time polymerase chain reactions (RT-PCR). The numbers of heme oxygenase-1 (*HO-1*) transcripts were normalized to *β-actin* amplified from the same sample and are presented as fold increase compared to control cells. Values are means ± SEM (N = 2, n = 4), $*p < 0.05$ relative to control. The trend analysis included controls.

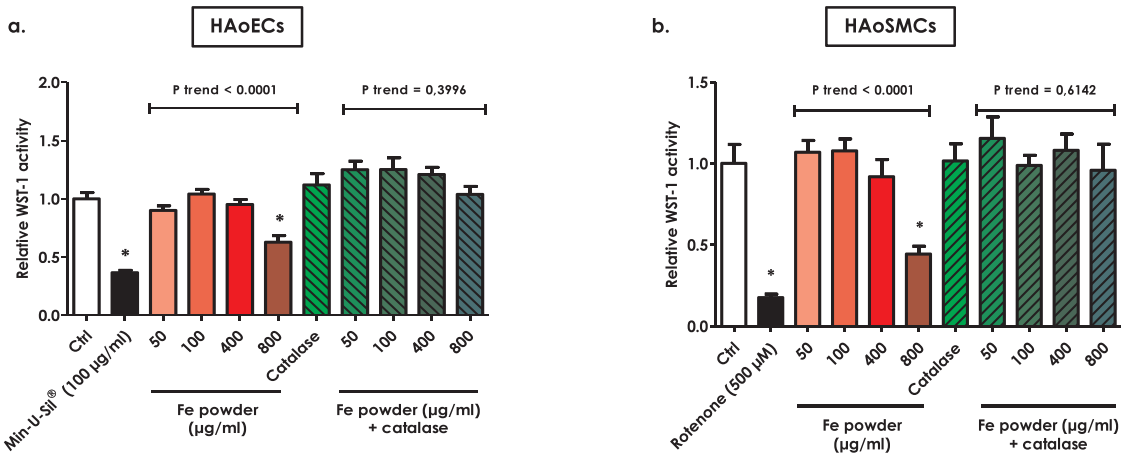

Fig. 6. HO• released during Fe powder corrosion affect ECs and SMCs viability. ECs (**a**: HUVECs; **b**: HAoECs) or SMCs (**c**: HCASMCs; **d**: HAoSMCs) were seeded in 96-well plate and exposed the day after to different concentrations of Fe powder for 24 h in the presence/absence of catalase (1000 U/ml). The cells were then washed and incubated in fresh medium with 10% WST-1 reagent for 2 h. Absorbance was measured at 450 nm, with 690 nm as reference, in a multiplate reader. Results are reported as relative WST-1 activity, where 1.0 corresponds to the value measured in untreated control cultures. Min-U-Sil® 5 or rotenone were used as positive controls. Values are means ± SEM (N = 4, n = 4), $*p < 0.05$ relative to control. The trend analysis included controls.

surrounding tissues. Tsaryk *et al.* [37] previously showed that endothelial cells might be subjected to ROS formed by electrochemical processes during Ti-based materials corrosion, but the implication of HO• produced by biodegradable Fe-based materials had not been investigated yet. Fagali *et al.* [18] showed that cells in direct contact with Fe particles expressed intracellular ROS.

In the present work we show that HO• generated during Fe corrosion induce oxidative stress in both ECs and SMCs and impair cell viability. The implication of HO• in the deleterious response of human ECs and SMCs, in the oxidative stress or cytotoxicity, was confirmed by the protective role of catalase. It is reasonable to assume that similar phenomena also occur *in vivo*. Indeed, the local corrosion of Fe implants releases Fe^{2+} ions that undergo the Fenton reaction in presence of H_2O_2, present in the tissue in response to wounding and inflammation, or mainly produced at the surface of the materials through the reaction of ferrous iron with oxygen. This oxidative microenvironment around the implant can lead to accelerated corrosion of the implant and further generation of metallic debris and ions [38]. As corrosion persists through the whole life of the stent, HO• are likely to be continuously formed at the implant site, progressively worsening the local oxidative stress already present in the diseased tissue. This mechanism could influence the success of the implantation and the healing of the surrounding tissues [36]. Information on oxidative stress is missing in the majority of existing *in vivo* experiments as investigators mostly looked at systemic toxicity rather than local toxicity, or they locally evaluated overt toxicity through histopathology analysis. With the present work, we provide a better understanding of the chemical and biological mechanisms involved in the cellular response to Fe-based implants and all these aspects should be considered during the development and evaluation of new Fe-based materials.

4.3. Strengths and limitations

The present *in vitro* model is simple but robust to easily assess the cytocompatibility of Fe-based materials. We demonstrated *in vitro* a fundamental mechanism behind Fe corrosion toxicity, and we identified

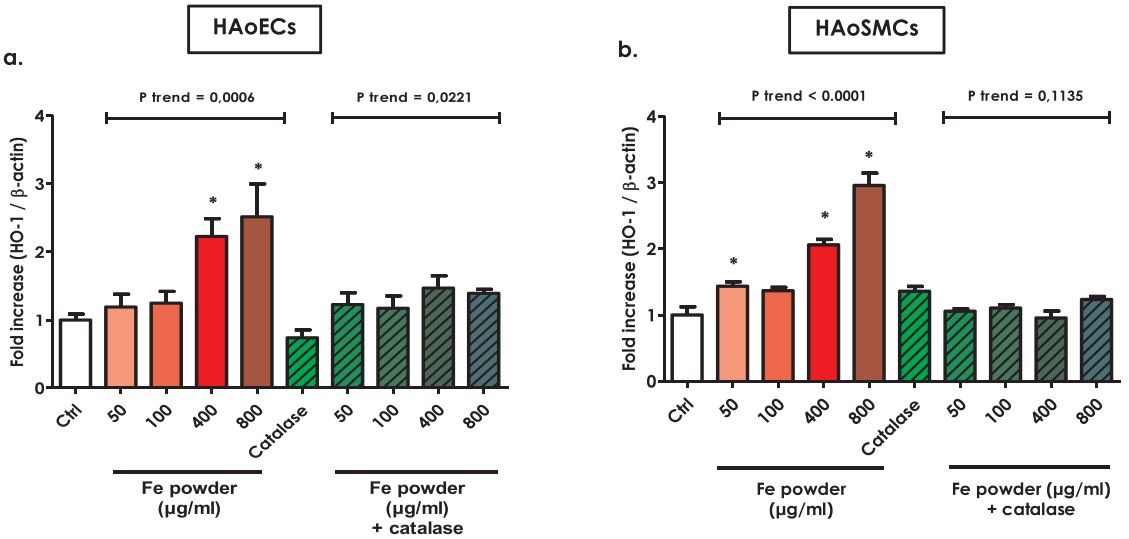

Fig. 7. HO• released from the corrosion of Fe powder induce oxidative stress in ECs and SMCs. ECs (**a**: HUVECs; **b**: HAoECs) or SMCs (**c**: HCASMCs; **d**: HAoSMCs) were exposed to different concentrations of Fe powder in the presence/absence of catalase (1000 U/ml) for 4 h (ECs) or 6 h (SMCs). RNA was extracted and reverse transcribed for real-time polymerase chain reactions (RT-PCR). The numbers of heme oxygenase-1 (*HO-1*) transcripts were normalized to *β-actin* amplified from the same sample and are presented as fold increase compared to untreated cells. Values are means ± SEM (N = 2, n = 4), $*p < 0.05$ relative to control. The trend analysis included controls.

the exact nature of the agent that contributes to oxidative stress generated by Fe degradation using catalase. The work covers different human cell lines to mimic the different stages occurring during the artery remodeling from the initial stent implantation to the complete degradation of the material. This experimental design can be extended to other transition metals, such as Co, that share redox properties and Fenton reactivity with Fe.

This study uses healthy human cell lines and this is limiting since a cardiovascular stent aims to support the healing process of a diseased tissue. Assessing the impact of Fe corrosion on endothelial and SM cells from patients with coronary disease or on cells from *e.g.* ApoE mice which develop atherosclerosis might deliver more realistic results [39]. However, we can expect that the oxidative stress and toxicity caused by Fe corrosion would be amplified under these pathological conditions.

5. Conclusion

The mechanisms highlighted here reveal a new aspect of the biodegradation of a Fe-based implant and its impact on surrounding tissues. Although several studies have concluded on the cytocompatibility of Fe-based materials [12,13], the direct interaction between materials and cells had seldom been explored. The present data indicate that some of the classical experiments used to evaluate biomaterials toxicity *in vitro*, such as exposure to soluble products, are not sufficient to capture the impact of implanted biodegradable Fe-based materials on surrounding tissue. The implication of HO• in the oxidative stress response and decreased cell viability in both human ECs and SMCs was confirmed by the protecting role of catalase. In addition, the present data indicate that oxidative stress might contribute to the toxicity of biodegradable Fe-based materials and this aspect appears particularly relevant for an atheromatous tissue already submitted to oxidative stress [40]. These findings should be considered for the assessment of the cytocompatibility of biodegradable Fe-based materials.

Author contributions

Designed and performed the experiments, and analyzed the data: ES. Performed the *in vitro* experiments on SMCs: AH. Designed and supervised the EPR experiments: MT and FT. Contributed metallic materials tools: PJJ. Designed and supervised the whole project: DL. Wrote the paper: ES and DL. All authors read and approved the final manuscript.

Declaration of Competing Interest

The authors declare no competing financial interest.

Acknowledgments

This work was supported by the “Communauté française de Belgique. Sections de Recherche Concertées” [contract 15/20-066] (principal promoter Pascal J. JACQUES).

Appendix A. Supplementary data

Supplementary material related to this article can be found, in the online version, at doi:https://doi.org/10.1016/j.colsurfb.2019.110542.

References

[1] J. Frostegard, Immunity, atherosclerosis and cardiovascular disease, BMC Med. 11 (117) (2013), https://doi.org/10.1186/1741-7015-11-117.
[2] H. Tomita, T. Nakanishi, K. Hamaoka, T. Kobayashi, Y. Ono, Stenting in congenital heart disease, Circ. J. 74 (8) (2010) 1676–1683, https://doi.org/10.1253/circj.CJ-10-0157.
[3] T. Huang, J. Cheng, Y.F. Zheng, In vitro degradation and biocompatibility of Fe-Pd and Fe-Pt composites fabricated by spark plasma sintering, Mater. Sci. Eng., C 35 (2014) 43–53, https://doi.org/10.1016/j.msec.2013.10.023.
[4] D. Williams, Concepts in biocompatibility: new biomaterials, new paradigms and new testing regimes, in: J.-P. Boutrand (Ed.), Biocompatibility and Performance of Medical Devices, Woodhead Publishing Series in Biomaterials, 2012, pp. 3–17.
[5] F.M. Tanja Kraus, S. Fischerauer, M. Fiedler, E. Martinelli, J. Eichler, F. Witte, E. Willbold, M. Schinhammer, M. Meischel, P.J. Uggowitzer, J.F. Löffler, A. Weinberg, Biodegradable Fe-based alloys for use in osteosynthesis: outcome of an in vivo study after 52 weeks, Acta Biomater. 10 (7) (2014) 3346–3353, https://doi.org/10.1016/j.actbio.2014.04.007.
[6] P.W.M. Peuster, M. Brügmann, M. Ehlerding, K. Seidler, C. Fink, H. Brauer, A. Fischer, G. Hausdorf, A novel approach to temporary stenting: degradable cardiovascular stents produced from corrodible metal—results 6–18 months after implantation into New Zealand white rabbits, Heart (London, U. K.) 86 (2001) 563–569, https://doi.org/10.1136/heart.86.5.563.
[7] R.P. Ron Waksman, Richard Baffour, Rufus Seabron, David Hellinga, Fermin O. Tio, Short-term effects of biocorrodible iron stents in porcine coronary arteries, J. Interv. Cardiol. 21 (1) (2008) 15–20, https://doi.org/10.1111/j.1540-8183.2007.00319.x.
[8] Q. Feng, D. Zhang, C. Xin, X. Liu, W. Lin, W. Zhang, S. Chen, K. Sun, Characterization and in vivo evaluation of a bio-corrodible nitrided iron stent, J. Mater. Sci. Mater. Med. 24 (3) (2013) 713–724, https://doi.org/10.1007/s10856-012-4823-z.
[9] Y.Y.A. Francis, S. Virtanen, A.R. Boccaccini, Iron and iron-based alloys for temporary cardiovascular applications, J. Mater. Sci. Mater. Med. 26 (3) (2015) 138, https://doi.org/10.1007/s10856-015-5473-8.
[10] D. Pierson, J. Edick, A. Tauscher, E. Pokorney, P. Bowen, J. Gelbaugh, J. Stinson, H. Getty, C.H. Lee, J. Drelich, J. Goldman, A simplified in vivo approach for evaluating the bioabsorbable behavior of candidate stent materials, J. Biomed. Mater. Res. Part B 100 (1) (2012) 58–67, https://doi.org/10.1002/jbm.b.31922.
[11] C.Y. Tingzhang Hu, Song Lin, Qingsong Yu, Guixue Wang, Biodegradable stents for coronary artery disease treatment: recent advances and future perspectives, Mater. Sci. Eng., C 91 (2018) 163–178, https://doi.org/10.1016/j.msec.2018.04.100.
[12] A.P.H. Hermawan, D. Dube, J. Couet, D. Mantovani, Fe–Mn alloys for metallic biodegradable stents: degradation and cell viability studies, Acta Biomater. 6 (2010) 1852–1860, https://doi.org/10.1016/j.actbio.2009.11.025.
[13] T. Huang, J. Cheng, D. Bian, Y. Zheng, Fe-Au and Fe-Ag composites as candidates for biodegradable stent materials, J. Biomed. Mater. Res. Part B 104 (2) (2016) 225–240, https://doi.org/10.1002/jbm.b.33389.
[14] W.R. Zhou, Y.F. Zheng, M.A. Leeflang, J. Zhou, Mechanical property, biocorrosion and in vitro biocompatibility evaluations of Mg-Li-(Al)-(RE) alloys for future cardiovascular stent application, Acta Biomater. 9 (10) (2013) 8488–8498, https://doi.org/10.1016/j.actbio.2013.01.032.
[15] I.G.M. Schinhammer, A.C. Hänzi, P.J. Uggowitzer, On the cytocompatibility of biodegradable Fe-based alloys, Mater. Sci. Eng. C 33 (2013) 782–789, https://doi.org/10.1016/j.msec.2012.11.002.
[16] Y.F.Z.B. Liu, Liquan Ruan, In vitro investigation of Fe30Mn6Si shape memory alloy as potential biodegradable metallic material, Mater. Lett. 65 (2011) 540–543, https://doi.org/10.1016/j.matlet.2010.10.068.
[17] W. Lin, G. Zhang, P. Cao, D. Zhang, Y. Zheng, R. Wu, L. Qin, G. Wang, T. Wen, Cytotoxicity and its test methodology for a bioabsorbable nitrided iron stent, J. Biomed. Mater. Res. Part B 103 (4) (2015) 764–776, https://doi.org/10.1002/jbm.b.33246.
[18] N.S. Fagali, C.A. Grillo, S. Puntarulo, M.A. Fernandez Lorenzo de Mele, Is there any difference in the biological impact of soluble and insoluble degradation products of iron-containing biomaterials? Colloids Surf. B 160 (2017) 238–246, https://doi.org/10.1016/j.colsurfb.2017.09.032.
[19] M. Schinhammer, A.C. Hänzi, P.J. Uggowitzer, On the cytocompatibility of biodegradable Fe-based alloys, Mater. Sci. Eng. C 33 (2013) 782–789, https://doi.org/10.1016/j.msec.2012.11.002.
[20] C.R. Keenan, D.L. Sedlak, Factors affecting the yield of oxidants from the reaction of nanoparticulate zero-valent iron and oxygen, Environ. Sci. Technol. 42 (2008) 1262–1267, https://doi.org/10.1021/es7025664.
[21] C.R. Keenan, R. Goth-Goldstein, D. Lucas, D.L. Sedlak, Oxidative stress induced by zero-valent iron nanoparticles and Fe(II) in human bronchial epithelial cells, Environ. Sci. Technol. 43 (2009) 4555–4560, https://doi.org/10.1021/es9006383.
[22] J. Prousek, E. Palacková, S. Priesolová, L. Marková, A. Alevová, Fenton- and Fenton like AOPs for wastewater treatment: from laboratory- to-plant-scale application, Sep. Sci. Technol. 42 (2007) 1505–1520, https://doi.org/10.1080/01496390701290151.
[23] Y. Deng, R. Zhao, Advanced Oxidation Processes (AOPs) in wastewater treatment, Curr. Pollut. Rep. 1 (3) (2015) 167–176, https://doi.org/10.1007/s40726-015-0015-z.
[24] K.R.H. Idrissi, L. Ryelandt, D. Schryvers, P.J. Jacques, On the mechanism of twin formation in Fe–Mn–C TWIP steels, Acta Mater. 58 (7) (2010) 2464–2476, https://doi.org/10.1016/j.actamat.2009.12.032.
[25] S.A.O. Bouaziz, C.P. Scott, P. Cugy, D. Barbier, High manganese austenitic twinning induced plasticity steels: a review of the microstructure properties relationships, Curr. Opin. Solid State Mater. Sci. 15 (4) (2011) 141–168, https://doi.org/10.1016/j.cossms.2011.04.002.
[26] L.A.T.W.T. Wallace, Y. Liu, B.L. Cooper, D.S. Mckay, A.S.J. Bo Chen, Lunar dust nd lunar simulant activation and monitoring, Meteorit. Planet. Sci. 44 (7) (2009) 961–970, https://doi.org/10.1111/j.1945-5100.2009.tb00781.x.
[27] F. Turci, G. Alberto, G. Martra, B. Fubini, Free-radical chemistry as a means to evaluate lunar dust health hazard in view of future missions to the moon, Astrobiology 15 (5) (2015) 371–380, https://doi.org/10.1089/ast.2014.1216.
[28] R.A. Crane, T.B. Scott, Nanoscale zero-valent iron: future prospects for an emerging water treatment technology, J. Hazard. Mater. 211-212 (2012) 112–125, https://

doi.org/10.1016/j.jhazmat.2011.11.073.
[29] T. Harada, T. Yatagai, Y. Kawase, Hydroxyl radical generation linked with iron dissolution and dissolved oxygen consumption in zero-valent iron wastewater treatment process, Chem. Eng. J. (London, U. K.) 303 (2016) 611–620, https://doi.org/10.1016/j.cej.2016.06.047.
[30] D.Y.T. Campbell Rogers, J.C. Squire, E.R. Edelman, Balloon-artery interactions during stent placement. A finite element analysis approach to pressure, compliance, and stent design as contributors to vascular injury, Circ. Res. 84 (1999) 378–383, https://doi.org/10.1161/01.RES.84.4.378.
[31] A. Curcio, D. Torella, C. Indolfi, Mechanisms of smooth muscle cell proliferation and endothelial regeneration after vascular injury and stenting, Circ. J. 75 (6) (2011) 1287–1296, https://doi.org/10.1253/circj.CJ-11-0366.
[32] S.O. Marx, H. Totary-Jain, A.R. Marks, Vascular smooth muscle cell proliferation in restenosis, Circ.: Cardiovasc. Interventions 4 (1) (2011) 104–111, https://doi.org/10.1161/CIRCINTERVENTIONS.110.957332.
[33] J. Cheng, B. Liu, Y.H. Wu, Y.F. Zheng, Comparative in vitro study on pure metals (Fe, Mn, Mg, Zn and W) as biodegradable metals, J. Mater. Sci. Technol. (Shenyang, China) 29 (7) (2013) 619–627, https://doi.org/10.1016/j.jmst.2013.03.019.
[34] J.K. Jaroslav Čapek, D. Vojtěch, E. Jablonská, J. Lipovc, T. Ruml, Microstructural, mechanical, corrosion and cytotoxicity characterization of the hot forged FeMn30(wt.%) alloy, Mater. Sci. Eng. C 58 (2016) 900–908, https://doi.org/10.1016/j.msec.2015.09.049.
[35] N.H. Shengfa Zhu, L. Xua, Y. Zhang, H. Liu, H. Sun, Y. Leng, Biocompatibility of pure iron: in vitro assessment of degradation kinetics and cytotoxicity on endothelial cells, Mater. Sci. Eng. C 29 (2009) 1589–1592, https://doi.org/10.1016/j.msec.2008.12.019.
[36] P.-A. Mouthuy, S.G. Dakin, L. Milkovi, A. Cipak Gasparovi, A.J. Carr, N. Zarkovi, Biocompatibility of implantable materials: an oxidative stress viewpoint, Biomaterials 109 (2016) 55–68, https://doi.org/10.1016/j.biomaterials.2016.09.010.
[37] M.K. Roman Tsaryk, U. Hempel, D. Scharnweber, R.E. Unger, P. Dieter, C.J. Kirkpatrick, K. Peters, Response of human endothelial cells to oxidative stress on Ti6Al4V alloy, Biomaterials 28 (2007) 806–813, https://doi.org/10.1016/j.biomaterials.2006.09.033.
[38] E. Zhang, H. Chen, F. Shen, Biocorrosion properties and blood and cell compatibility of pure iron as a biodegradable biomaterial, J. Mater. Sci. Mater. Med. 21 (7) (2010) 2151–2163, https://doi.org/10.1007/s10856-010-4070-0.
[39] K.S. Meir, E. Leitersdorf, Atherosclerosis in the apolipoprotein-E-deficient mouse: a decade of progress, Arterioscler. Thromb. Vasc. Biol. 24 (6) (2004) 1006–1014, https://doi.org/10.1161/01.ATV.0000128849.12617.f4.
[40] K. Chen, J.F. Keaney Jr., Evolving concepts of oxidative stress and reactive oxygen species in cardiovascular disease, Curr. Atheroscler. Rep. 14 (5) (2012) 476–483, https://doi.org/10.1007/s11883-012-0266-8.